Invited Paper

On-chip graphene optoelectronic devices for high-speed modulation and photodetection

Ren-Jye Shiue[a], Xuetao Gan[b] and Dirk Englund[a]

[a]Department of Electrical Engineering and Computer Science, Massachusetts Institute of Technology, Cambridge, MA, United States;
[b]Department of Electrical Engineering, Columbia University, New York, NY, United States

ABSTRACT

There has been a rapidly growing interest in graphene-based optoelectronics. This exceptional material exhibits broadband optical response, ultrahigh carrier mobility and more importantly, potential compatibility with silicon complementary metal-oxide semiconductor (CMOS) technology. Here we present our recent works that integrate graphene with silicon channel waveguides and photonic crystal cavities. By coupling graphene to an optical cavity, we demonstrated an efficient electro-optic modulator that features a modulation depth of 10 dB and a switching energy of 300 fJ. Several high-speed modulators are also tested, showing a speed up to 0.57 GHz. In addition, we implemented a graphene photodetector on a silicon waveguide. The 53-μm-long graphene channel couples to the evanescent field of the waveguide mode, resulting in more than 60% absorption of the input light. We demonstrated a responsivity of 0.108 A/W in our photodetector. A data transmission of 12 Gbps and response time in excess of 20 GHz are also achieved. These results show the feasibility of graphene as a building block for silicon photonic integrated circuits. In particular, on-chip graphene active devices such as modulators and photodetectors are promising for their broadband response, high-speed operation, low power consumption and ease-to-fabrication.

Keywords: Graphene, Optoelectronics, Photodetector, Electro-optic modulator, Silicon photonics

1. INTRODUCTION

Optical interconnects have emerged as a promising solution for compact and fast communication links to replace current electrical interconnects. Silicon-based photonics is of particular attractive because it enables cost-effective integration of optics and electronics.[1,2] A major challenge in silicon-based photonics comes from a low electro-optic coefficient and an intrinsic band gap that is larger than the desired photon energy in telecommunication bands (1.3 μm $\sim$ 1.5 μm). To overcome these difficulties, a hybrid system of silicon and a second material with strong light-matter interaction could enhance the functionality of silicon photonics, providing a complete platform for extensive applications. Recently, graphene—a monolayer of hexagonally packed carbon atoms—has drawn attention for optoelectronic applications due to its remarkable optical and electronic properties. Strong light-matter interaction is theoretically predicted and experimentally observed from its unique linear band structure,[3] resulting in a uniform absorption coefficient of $\pi\alpha \sim 2.3\%$, where α is the fine structure constant.[4] This universal absorption of graphene persists in the spectral range from visible to mid-infrared, making it an ideal material for broadband applications. More importantly, the optical transition in graphene can be tuned by electrostatic gating,[5] providing an effective approach to control the absorption of graphene by static electric field. Combined with its notably high carrier mobility[6] and ultrafast carrier relaxation dynamics,[7] graphene-based optoelectronics exhibits considerable potential for high-speed optical links.[8–12]

Here, we present our recent works that integrate graphene with silicon channel waveguides and planar photonic crystal (PPC) cavities. As an active material in silicon-based photonics, we demonstrate that graphene is suitable for electro-optic modulators and photodetectors with high quality. Graphene's light-matter interaction can be enhanced by coupling the material to the evanescent field of a nanocavity.[13] The attenuation of the cavity reflection is amplified and controlled by the absorption of graphene. We have realized an electro-optic

Ren-Jye Shiue: E-mail: tedshiue@mit.edu

Photonic and Phononic Properties of Engineered Nanostructures IV, edited by Ali Adibi, Shawn-Yu Lin, Axel Scherer,
Proc. of SPIE Vol. 8994, 89940P · © 2014 SPIE · CCC code: 0277-786X/14/$18 · doi: 10.1117/12.2047906

modulator with a modulation depth of 10 dB and a switching energy of 300 fJ.[14] Moreover, several high-speed modulators are also implemented, showing a speed as high as 0.57 GHz.[15] On the other hand, the increased absorption of graphene in a cavity is explored for photodetection. We have shown a controlled enhancement of photoresponsivity in graphene photodetectors with a maximum eight-fold enhancement when the incident light is on resonant with the cavity field. Similar to the cavity coupled devices, the extended interaction length of graphene coupled to silicon waveguides provides strong enhancement of the absorption in graphene. We demonstrate a photodetector with a responsivity of 0.108 A/W for broadband photodetection.[16] The speed of the photodetector is higher than 20 GHz and a data transmission rate of 12 Gbps is tested for this chip-integrated graphene photodetector.

2. CAVITY-ENHANCED LIGHT-MATTER INTERACTION IN GRAPHENE

In optical cavities, the field intensity is proportional to Q/V_{mode}, where Q and V_{mode} are the quality factor and mode volume of the resonant mode, respectively. PPC nanocavities can have extremely high Q factor (up to 10^6) and ultrasmall V_{mode} (on the order of a cubic wavelength),[17] which makes them appealing for exploring strong light-matter coupling. When graphene couples to a PPC nanocavity, the cavity transmission, reflection and the absorption can be modeled by coupled mode theory.[13] As shown in Fig. 1(a), the cavity couples with a waveguide through the forward and backward propagating modes at rates of κ_{ca} and κ_{cb}. The loss of the unloaded cavity has a decay rate of $\kappa_c = \omega_0/Q$, where ω_0 is the angular frequency of the cavity resonance. Graphene causes additional loss in the cavity by an energy decay rate κ_{cg}, together with a frequency shift $\Delta\omega$ in the cavity resonance. In our experiments, the cavity-graphene system is characterized by a cross-polarization confocal microscopy. Therefore, the excitation mode $a+$ and the collection mode $b-$ are approximately Gaussian spatial modes, given by the optics of the confocal microscope. Due to the symmetric confinement, we assume the resonant mode of the PPC cavity decays equally into forward and backward modes, i.e. $\kappa_{ca} = \kappa_{cb}$. A coupling efficiency η between the microscope modes and the cavity radiation is introduced so that the cavity mode couples with the microscope modes with rates $\eta\kappa_c = \kappa_{ca} = \kappa_{cb}$. We solve the steady-state solution to the coupled mode equation to extract the frequency dependent reflection $R_g(\omega)$ and absorption $A_g(\omega)$, giving

$$R_g(\omega) = \frac{\eta^2\kappa_c^2}{(\omega_0 + \Delta\omega - \omega)^2 + (\kappa_c/2 + \kappa_{cg}/2)^2} \tag{1}$$

$$A_g(\omega) = \frac{\eta\kappa_c\kappa_{cg}}{(\omega_0 + \Delta\omega - \omega)^2 + (\kappa_c/2 + \kappa_{cg}/2)^2} \tag{2}$$

From above expressions of the cavity reflection R_g and graphene absorption A_g, we can easily deduce the effect of the interaction between graphene and the localized cavity mode with respect to the ratio κ_c/κ_{cg}, as shown in Fig. 1(b). The blue curve shows the reflectivity attenuation of the cavity at the frequency of ω_0, defined as $10\log_{10}(R_{intrinsic}(\omega_0)/R_{graphene}(\omega_0))$, versus κ_c/κ_{cg}. The attenuation ratio for the reflectivities with and without graphene vary as $(1 + \kappa_{cg}/\kappa_c)^2$, indicating that the reflectivity of the graphene-cavity system can be dramatically modulated by altering the parameter κ_c/κ_{cg}. For a high-Q cavity ($Q \sim 2,600$), even the small absorption due to a monolayer of graphene can result in a transmission loss as high as 20 dB.[13] The graphene absorbance at the frequency of $\omega_0 + \Delta\omega$ versus κ_c/κ_{cg} is shown in the green curve of Fig. 1(b). Unlike the modulation of the cavity reflection, the on-resonance absorbance of graphene has a maximum value of κ_{ca}/κ_c, which is reached by optimizing the system decay rates to satisfy $\kappa_{cg} = \kappa_c$. This critical coupling condition indicates that matching the graphene-induced loss to the intrinsic cavity loss yields maximal absorbance in graphene. In general, the cavity resonance has the same forward and backward coupling rate, i.e. $\kappa_{ca} = \kappa_{cb}$. The maximum absorbance in graphene can reach 50% if the waveguide-cavity coupling is responsible for the entire intrinsic loss of the cavity. However, in cavities having the traveling-wave resonant mode, such as ring resonators,[18] there is no backward coupling, which enables maximum absorbance of 100% in graphene.

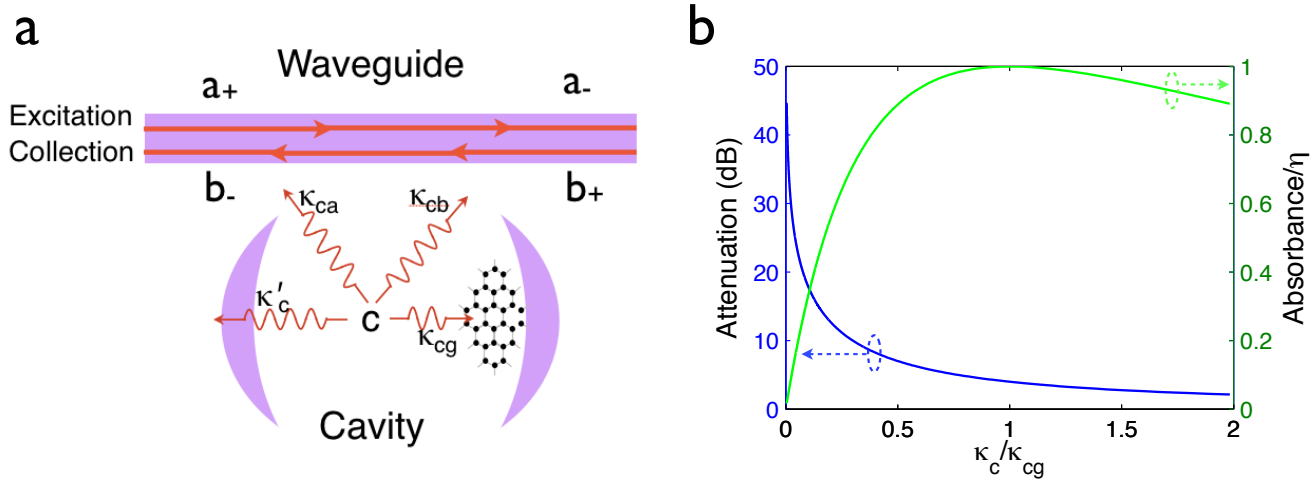

Figure 1. (a) Coupled mode theory for graphene in a cavity. The cavity intrinsic field c couple to the forward ($a\pm$) and backward ($b\pm$) modes of a waveguide. The cavity has an intrinsic loss rate κ_c and graphene induces excess loss κ_{cg} in the cavity. (b) Attenuation and normalized absorbance versus κ_c/κ_{cg} calculated using a coupled graphene-cavity model

3. GRAPHENE-BASED OPTOELECTRONICS INTEGRATED WITH A PPC CAVITY

Based on cavity-enhanced light-matter interaction in graphene, we implement graphene electro-optic modulators and photodetectors. For modulators, the reflection of the cavity is monitored and varied by tuning the chemical potential μ (also Fermi level E_F) of graphene. The intensity of the cavity reflection drastically increases when the Fermi energy E_F reaches half of the incident photon energy, i.e. $E_F = \frac{1}{2}\hbar\omega$. In this case, optical transitions are inhibited in the Paul blocking regime.[14] We study the d.c. response of the cavity reflection as well as the dynamic response of the light modulation at high speed. For photodetection, a multimode cavity is integrated with a graphene photodetector. The coupling between the cavity and graphene for enhanced photocurrent generation is both analyzed theoretically and characterized experimentally. A maximum enhancement factor of eight is achieved with a optimized coupling condition of $\kappa_c/\kappa_{cg} \approx 1.3$.

3.1 High-contrast Graphene Electro-optic Modulators

Fig. 2(a) shows the scheme of the graphene electro-optic modulator. An air-slot PPC nanocavity was fabricated on a silicon-on-insulator wafer with a 220 nm thick silicon membrane using a series of electron-beam lithography and dry/wet etching steps. After graphene was transferred on top of the PPC cavity, source, drain and gate metal electrodes were defined by e-beam lithography, metal deposition and lift-off. Finally, an electrolyte (PEO plus LiClO4) layer was spun on the entire wafer, serving to induce high electrical fields and carrier densities on the surface of graphene. The optical transmission of the monolayer graphene can be modulated by electrostatistically tuning the Fermi energy (E_F) of graphene, as illustrated in Fig. 2(b) When the incident photo energy $\hbar\omega$ is lower than twice of the Fermi energy E_F away from the charge neutrality point (Dirac point), inter-band transition of valence electrons are essentially blocked by Pauli principle.[4,14] Therefore, in the Pauli-blocking regime, the absorption of graphene is largely reduced, giving a sharp transition of the cavity reflectivity and the Q factor. By tuning the Fermi level with electrolyte gating, we can electrically modulate the cavity reflection efficiently.

We characterized the graphene-PPC nanocavity using a cross-polarization confocal microscope with a broadband (super-continuum laser) excitation source. The cavity reflection was analyzed using a commercial spectrometer with a resolution 0.05 nm. The measured optical and electrical signal were recorded simultaneously and presented in Fig. 3. We swept the gate voltage in a sawtooth pattern between -7 V and 6 V. The resistance peak in Fig. 3(b) indicates the charge neutrality point (V_{CN}) of our graphene field effect transistor (FET), which is at $V_{CN} = 1$ V. In Fig. 3(c), three different resonant modes are evolving as the gate voltage V_G is sweeping. At $V_G = 0$ to -1 V, the cavity spectrum remains unchanged. Two peaks can be observed at the wavelengths of

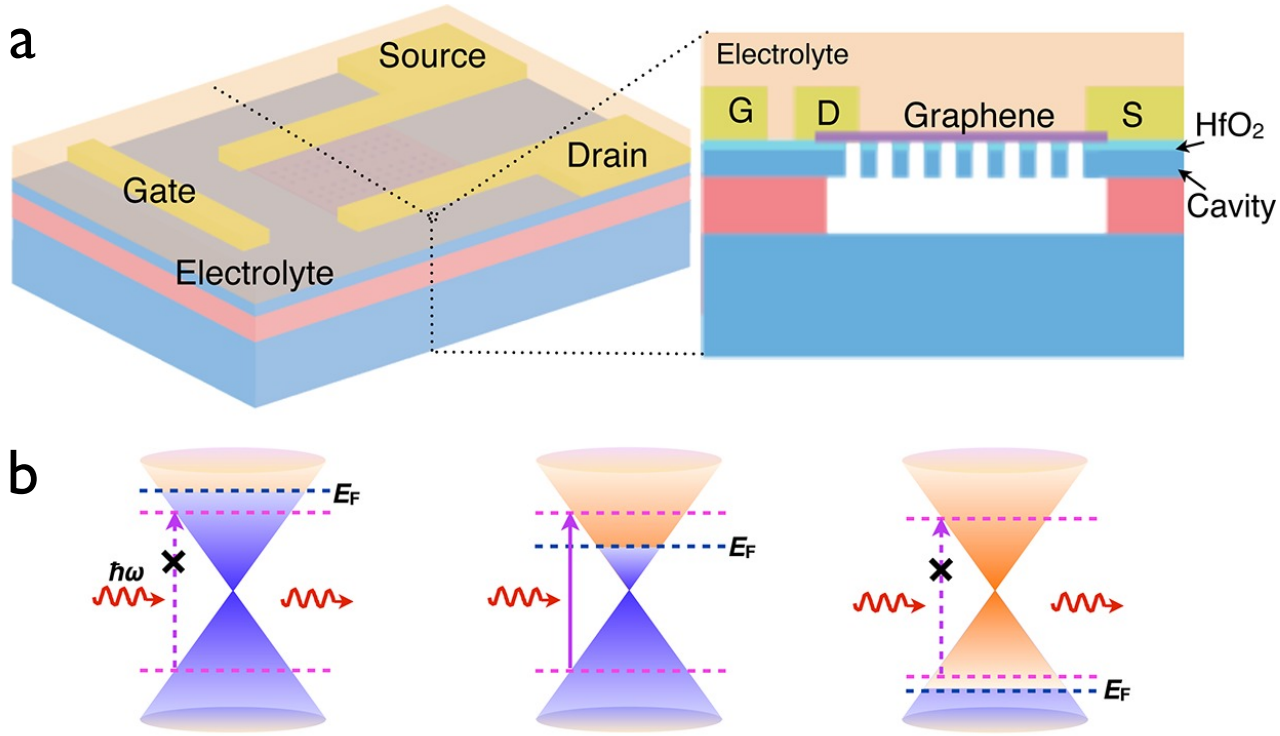

Figure 2. (a) Schematic of the PPC cavity-integrated graphene modulator. (b) Band structure of graphene. The inter-band transition are suppressed in graphene at high doping level and the graphene becomes more transparent as a result of Pauli blocking.

1571.1 nm and 1593 nm, respectively (top panel of Fig. 3(d)). As V_G goes below -1 V, the two peaks narrow and red shift slightly. The increase of cavity reflectivity arises from the reduction of graphene absorption, where Pauli blocking starts to take effect. Decreasing V_G further, the peaks continue to grow narrow but start to blue shift. The Q factor stabilizes when V_G is below -2.5 V, indicating the Pauli blocking regime. At V_G = -7 V, these peaks are very narrow and a mode at 1576 nm becomes more distinguishable (third panel of Fig. 3(d)). The cavity spectrum shows corresponding behaviors when V_G is moving back from -7 V to 0 V. At positive V_G, graphene becomes n doped when V_G is larger than V_{CN}. The evolution of the cavity spectrum has the same effects for the n- and p-doped sides of graphene and is therefore symmetrical to V_{CN} = 1 V. We extract a maximum of 10 dB in modulation depth when a narrow band laser of 1592.9 nm was used for input and a voltage swing of -1.75 ± 0.75 V was applied to drive the modulator. The variation of the Q and the cavity reflection satisfy the coupled mode theory, the numerical simulation of the cavity modes and the optical conductivity of graphene based on inter- and intraband transitions.[14] Considering the capacitor area built in this device (30 μm^2), the switch energy is about 300 fJ. However, the capacitor area can be optimized to as small as the defect region in the PPC cavity, which is smaller than 0.5 μm^2. In this case, the power consumption can be reduced below 1 fJ per bit.

3.2 High-speed Graphene-cavity Modulator

For modulators gated by ionic electrolyte, the speed of the device is limited by the mobile ions in the electrolyte. Therefore, the modulator introduced in last paragraph does not allow gigahertz operations. To realize a high-speed modulator, alternatively, we fabricated a hybrid graphene-silicon modulator according to the scheme illustrated in Fig. 4(a). A graphene capacitor consisting of two graphene monolayers were separated by a boron nitride (BN) dielectric layer. This dual-gated graphene capacitor was then transferred onto a PPC cavity on the SOI substrate. A hafnium oxide (HfO_2) layer was deposited between the silicon surface and the bottom graphene before transfer to electrically isolate silicon and graphene. Finally contact electrodes were deposited

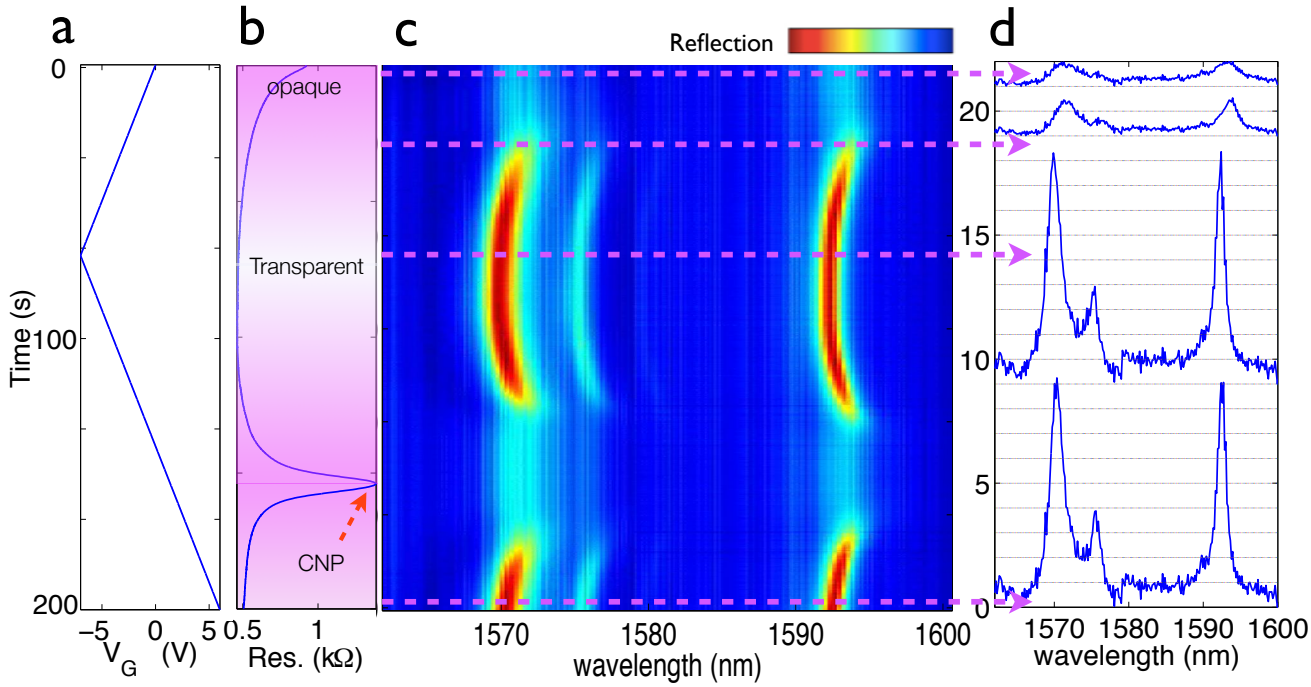

Figure 3. Electrical and optical response of the graphene-PPC nanocavity modulator. (a) Gate voltage (V_G) as a function of time. (b) Resistance of the graphene FET. (c) Reflection spectra of the cavity as V_G is modulated. Three resonant peaks show clear shift in wavelengths and modulation in intensity and Q factors as the V_G is adjusted. (d) Normalized spectra of the cavity reflectivity in (c) at $V_G = 0$, -1, -7 and 6 V (top to button).

on the dual-layer graphene capacitor by e-beam lithography, metal evaporation and lift-off. An optical image of as-fabricated device is displayed in Fig. 4(b). When a bias voltage V_G is applied across the two graphene layers, the two graphene plate conductors are doped with similar Fermi level and reach optical transparency simultaneously. The reduction of the absorption of the dual graphene layers enables more efficient modulation of the cavity reflection. We characterized the frequency dependent modulation of the cavity reflection by sweeping a narrow band input laser from 1510 nm to 1530 nm. The voltage swing was kept at 1.25 ± 1.25 V with a modulation frequency of 100 kHz and the cavity reflection was measured using a fast InGaAs photoreceiver. As shown in Fig. 4(c), the modulation depth is maximized when the input laser is on resonant with the cavity mode. The maximum modulation depth of 1.5 dB is achieved. Due to the a smaller capacitor comparing to the electrolyte-gated device, the dual-layer graphene modulator exhibits lower modulation depth. However, the magnitude of modulation can be further improved by using a thinner BN insulating layer or a cavity that operates at a lower resonant frequencies.[15] We then tested the a.c. response of the dual-layer graphene modulator at a speed from 20 MHz to 2 GHz. Fig. 4(d) shows the normalized response of the modulation depth as a function of frequency. The 3-dB cutoff frequency of the device is about 0.57 GHz. We attribute the limited speed of our device to a large RC constant, which is consistent with the calculated and measured electrical properties of the device.[15]

3.3 Cavity-integrated Graphene Photodetector with Enhanced Responsivity

The cavity-enhanced absorption in graphene could also be facilitated to make efficient photodetectors in silicon photonics. Here we implement a graphene photodetector coupled to a multimode PPC cavity. As shown in Fig. 5(a), a PPC cavity was designed by introducing a linear defect in the middle of the PPC lattice. Monolayer graphene was transfer on top of the cavity and the metal electrodes were fabricated with the same technique described previously. In Fig. 5(b), we plot the cavity resonance before (blue) and after (red) graphene is deposited. Multiple resonant peaks are observed in the blue curve for unloaded cavity. After graphene is transferred, the resonant peaks are broadened and the intensity of cavity reflection is attenuated, consistent with

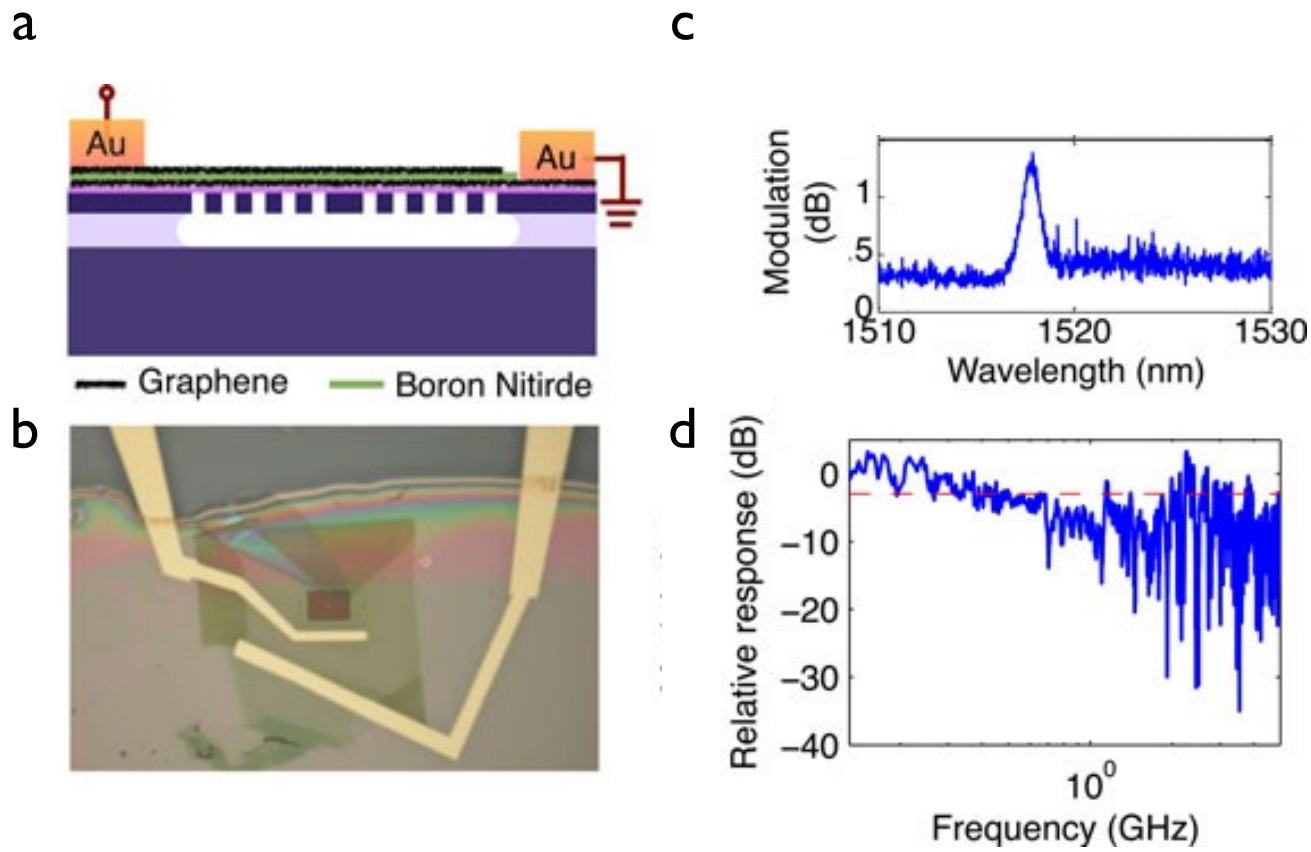

Figure 4. (a) Schematic of the high-speed graphene modulator based on dual graphene layers. (b) Optical microscope image of a fabricated device. (c) Spectrally resolved modulation of the device shown in (b). (d) Dynamics response of the modulator.

the theory when excess loss of graphene is introduced in the cavity. We tested the photodetector with a tunable CW laser modulated at a frequency of 20 kHz. Due to the absence of junctions on the graphene channel, we applied a d.c. bias voltage across the source and drain electrodes to separate the photoexcited carriers. The a.c. photocurrent was fed into a current preamplifier and read by a lock-in amplifier. Fig. 5(c) shows the photocurrent spectra (blue) of the cavity-integrated graphene photodetector. Multiple peaks in the photocurrent spectra are observed, which is similar to the reflection spectra in Fig. 5(b). To understand the measured spectra, we use the parameters of cavity intrinsic loss κ_c, graphene-induced excess loss κ_{cg} and the resonant frequency ω of the cavity modes extracted from the cavity reflection in Fig. 5(b) using the coupled mode theory,[19] and calculate the absorption in graphene as a function of input wavelengths. The purple dashed curve in Fig. 5(d) displays the calculated absorption spectra of graphene, showing good agreed with the experimentally measured results (blue). In this device, a maximum of eight-fold enhancement in photocurrent is achieved when the light is on resonance with the cavity modes.

4. BROADBAND GRAPHENE PHOTODETECTOR WITH HIGH RESPONSIVELY FOR SILICON PHOTONICS

Cavity-enhanced graphene optoelectronics is able to enhance light-matter interaction in sub-micron length scale, enabling a way to design efficient devices with small footprint and low power consumption. However, for broadband applications, we integrated graphene with waveguides rather than cavities. Fig. 6(a) shows the scheme of the waveguide-integrated graphene photodetector. A 53-μm-long graphene sheet was deposited on a silicon channel waveguide. Two metal electrical leads were placed on top of graphene to extract photocurrent. As

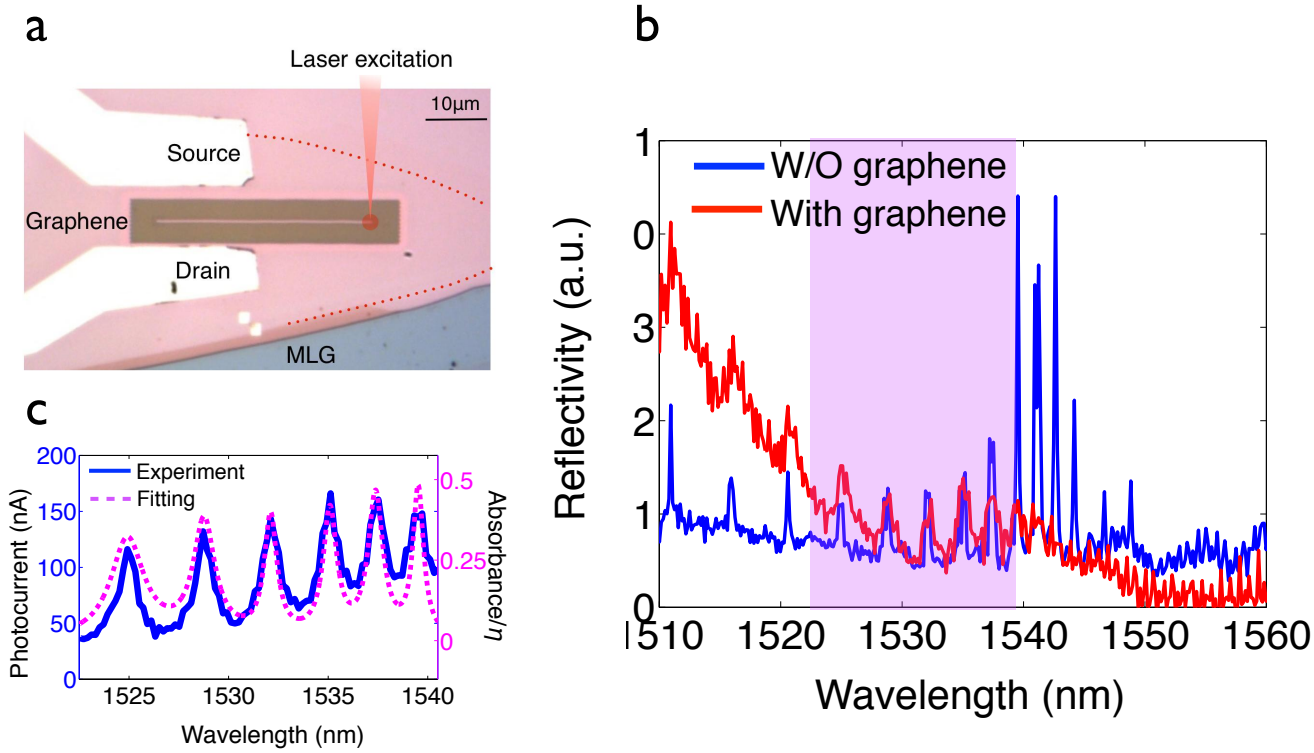

Figure 5. (a) An optical image of the cavity-integrated graphene photodetector. (b) Reflection spectra of the PPC cavity before (blue) and after (red) graphene deposition. (c) Photocurrent spectra of the detector (blue) and the normalized absorption spectra (purple) in graphene predicted by the coupled mode theory.

the optical image shown in Fig. 6(b), we designed the contact geometry so that one side of the metal contacts was placed within a distance of 200 nm away from the edge of the waveguide. Because of the intrinsic doping caused by metal on top of graphene, a built in electrical field is induced around the metal/graphene interface, as illustrated in Fig. 6(c). This built-in electric field serves to increase the quantum efficiency of the photodetector. Together with the enhanced absorption length of graphene on waveguide, we observed a total of 60% absorption in our graphene detector, consistent with the numerical simulations using finite element methods.[16] The responsivity achieved 0.108 mA/W with a spectral bandwidth over 140 nm (1450 nm $\sim$ 1590 nm). Unlike conventional semiconductors, both electrons and holes in graphene exhibits very high mobility ($\sim 10,000$ cm^2/Vs), and a moderate internal electric field would be sufficient to separate photocarriers efficiently. We examined the high-speed response of the device using a commercial lightwave component analyzer (LCA) with a frequency range from 0.13 GHz to 20 GHz. A modulated optical signal at a wavelength of 1550 nm with an average power of 1 mW emitted from the LCA was coupled into the device and the electrical output was extracted through a ground-source (G-S) RF microwave probe and fed back into the electrical port of the LCA. We observed only 1 dB degradation of the signal magnitude at 20 GHz. To gauge the viability of the waveguide-integrated graphene photodetector in a realistic optical link, we performed a test of optical data transmission. A pulsed pattern generator with a maximum 12 Gbit/s internal electrical bit stream modulated an 1550 nm CW laser via a lithium niobate (LiNbO3) electro-optic modulator, which was launched into the waveguide-integrated graphene detector. The output electrical data stream from the graphene detector was amplified and sent to a wide-band oscilloscope to obtain an eye diagram. As shown in the inset of Fig. 6(d), a clear eye-opening diagram at 12 Gbit/s was obtained.

5. CONCLUSIONS

Graphene exhibits great potential for a wide range of photonic and optoelectronic applications. The integration of graphene with existing silicon-based photonics can strongly enhance the light-matter interaction in graphene

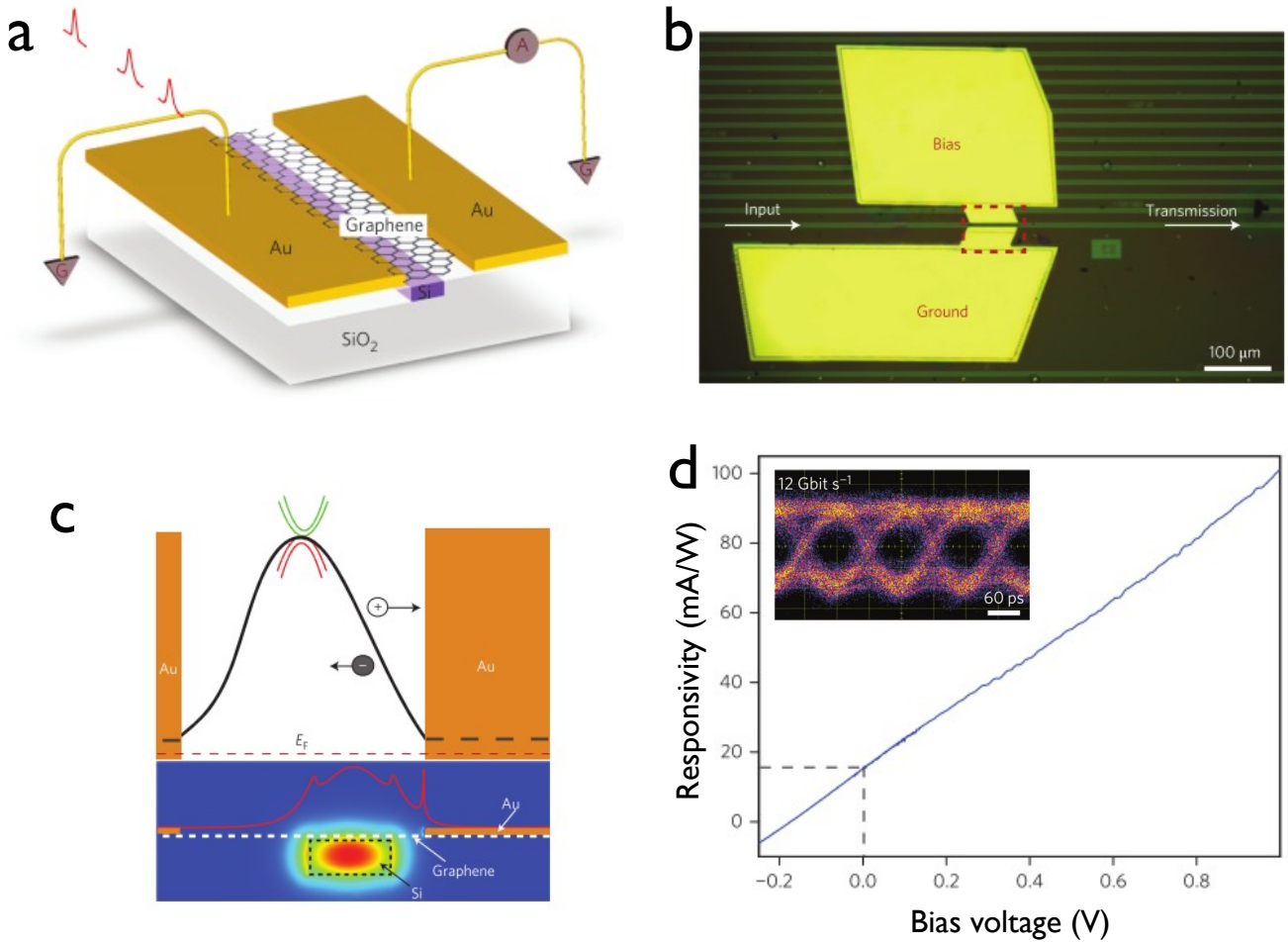

Figure 6. (a) Schematic of a waveguide integrated graphene photodetector. (b) Optical image of the graphene photodetector on top of the silicon waveguide (c) Illustration of the potential difference across the graphene channel (top). A built-in electric field overlaps with optical field that couples to graphene, serving to separate light generated electron-hole pair on the graphene surface. (d) The response of the waveguide-integrated graphene photodetector as a function of source-drain bias voltage (V_{DS}). The highest responsivity at $V_{DS} = 1$ V is 0.108 mA/W. Inset: An eye diagram acquired using the graphene photodetector in a 12 Gbit/s optical data link.

for efficient optoelectronic devices. Moreover, graphene provides an ideal active material to complement the functionality of silicon-based photonics. Compared to many traditional active materials that have been integrated into silicon, graphene promises relative ease of fabrication, compact footprint, ultrafast carrier transport dynamics and low power consumption. The photodetectors and modulators described here are potentially compatible with CMOS processes. The PPC cavity-integrated modulators can in principle be coupled with a lateral PPC waveguide in a fully integrated photonic chip for fiber-based optical links. Large-scale production and transfer of graphene sheets have also been demonstrated by several groups.[20,21] We expect that a fully CMOS compatible integration of silicon with graphene would be possible in the near future, leading to a promising hybrid platform for compact and high-speed photonic integrated circuits.

ACKNOWLEDGMENTS

This work was supported in part by the Center for Excitonics, an Energy Frontier Research Center funded by the U.S. Department of Energy, Office of Science, Office of Basic Energy Sciences under Award No. DE-SC0001088. Device fabrication was carried out at the Center for Functional Nanomaterials, Brookhaven National Laboratory, which was supported by the U.S. Department of Energy, Office of Basic Energy Sciences, under Contract No. DE- AC02-98CH10886. Graphene assembly was supported by the Center for Re-Defining Photovoltaic Efficiency Through Molecule Scale Control, an Energy Frontier Research Center funded by the U.S. Department of Energy, Office of Science, Office of Basic Energy Science under Award No. DE-SC0001085.

REFERENCES

[1] Soref, R., "The past, present, and future of silicon photonics," *Selected Topics in Quantum Electronics, IEEE Journal ...* **12**(6), 1678–1687 (2006).

[2] Jalali, B. and Fathpour, S., "Silicon Photonics," *Journal of Lightwave Technology* **24**, 4600–4615 (Dec. 2006).

[3] Castro Neto, a. H., Peres, N. M. R., Novoselov, K. S., and Geim, a. K., "The electronic properties of graphene," *Reviews of Modern Physics* **81**, 109–162 (Jan. 2009).

[4] Mak, K. F., Sfeir, M. Y., Wu, Y., Lui, C. H., Misewich, J., and Heinz, T. F., "Measurement of the Optical Conductivity of Graphene," *Physical Review Letters* **101**(19), 196405 (2008).

[5] Li, Z. Q., Henriksen, E. a., Jiang, Z., Hao, Z., Martin, M. C., Kim, P., Stormer, H. L., and Basov, D. N., "Dirac charge dynamics in graphene by infrared spectroscopy," *Nature Physics* **4**, 532–535 (June 2008).

[6] Dean, C. R., Young, a. F., Meric, I., Lee, C., Wang, L., Sorgenfrei, S., Watanabe, K., Taniguchi, T., Kim, P., Shepard, K. L., and Hone, J., "Boron nitride substrates for high-quality graphene electronics.," *Nature nanotechnology* **5**, 722–6 (Oct. 2010).

[7] Sun, D., Aivazian, G., Jones, A. M., Ross, J. S., Yao, W., Cobden, D., and Xu, X., "Ultrafast hot-carrier-dominated photocurrent in graphene," **7**(February) (2012).

[8] Liu, M., Yin, X., Ulin-Avila, E., Geng, B., Zentgraf, T., Ju, L., Wang, F., and Zhang, X., "A graphene-based broadband optical modulator.," *Nature* **474**(7349), 64–67 (2011).

[9] Bao, Q. and Loh, K. P., "Graphene photonics, plasmonics, and broadband optoelectronic devices.," *ACS nano* **6**(5), 3677–3694 (2012).

[10] Avouris, P. and Freitag, M., "Graphene Photonics, Plasmonics, and Optoelectronics," *IEEE Journal of Selected Topics in Quantum Electronics* **20**, 6000112–6000112 (Jan. 2014).

[11] Bonaccorso, F., Sun, Z., Hasan, T., and Ferrari, A. C., "Graphene photonics and optoelectronics," *Nature Photonics* **4**, 611–622 (Aug. 2010).

[12] Mueller, T., Xia, F., and Avouris, P., "Graphene photodetectors for high-speed optical communications," *Nature Photonics* **4**, 297–301 (Mar. 2010).

[13] Gan, X., Mak, K. F., Gao, Y., You, Y., Hatami, F., Hone, J., Heinz, T. F., and Englund, D., "Strong Enhancement of Light-Matter Interaction in Graphene Coupled to a Photonic Crystal Nanocavity.," *Nano letters* **12**, 5626 (Oct. 2012).

[14] Gan, X., Shiue, R.-J., Gao, Y., Mak, K. F., Yao, X., Li, L., Szep, A., Walker, D., Hone, J., Heinz, T. F., and Englund, D., "High-contrast electrooptic modulation of a photonic crystal nanocavity by electrical gating of graphene.," *Nano letters* **13**, 691–6 (Mar. 2013).

[15] Gan, X., Shiue, R.-j., Gao, Y., Assefa, S., Hone, J., and Englund, D., "Controlled light-matter interaction in graphene electro-optic devices using nanophotonic cavities and waveguides," **20**(1) (2014).

[16] Gan, X., Shiue, R.-J., Gao, Y., Meric, I., Heinz, T. F., Shepard, K., Hone, J., Assefa, S., and Englund, D., "Chip-integrated ultrafast graphene photodetector with high responsivity," *Nature Photonics* **7**, 883–887 (Sept. 2013).

[17] Akahane, Y., Asano, T., Song, B.-S., and Noda, S., "Fine-tuned high-Q photonic-crystal nanocavity," *Optics Express* **13**(4), 1202–1214 (2005).

[18] Manolatou, C., Khan, M., Fan, S., Villeneuve, P., Haus, H., and Joannopoulos, J., "Coupling of modes analysis of resonant channel add-drop filters," *IEEE Journal of Quantum Electronics* **35**(9), 1322–1331 (1999).

[19] Shiue, R.-J., Gan, X., Gao, Y., Li, L., Yao, X., Szep, A., Walker, D., Hone, J., and Englund, D., "Enhanced photodetection in graphene-integrated photonic crystal cavity," *Applied Physics Letters* **103**(24), 241109 (2013).

[20] Bae, S., Kim, H., Lee, Y., Xu, X., Park, J.-S., Zheng, Y., Balakrishnan, J., Lei, T., Kim, H. R., Song, Y. I., Kim, Y.-J., Kim, K. S., Ozyilmaz, B., Ahn, J.-H., Hong, B. H., and Iijima, S., "Roll-to-roll production of 30-inch graphene films for transparent electrodes.," *Nature nanotechnology* **5**, 574–8 (Aug. 2010).

[21] Gao, L., Ni, G.-X., Liu, Y., Liu, B., Castro Neto, A. H., and Loh, K. P., "Face-to-face transfer of wafer-scale graphene films.," *Nature* **505**, 190–194 (Dec. 2013).